Archives of Hydro-Engineering and Environmental Mechanics
Vol. 58 (2011), No. 1–4, pp. 23–45
DOI: 10.2478/v10203-011-0002-9

Simulation of Solitary Wave Mechanics by a Corrected Smoothed Particle Hydrodymamics Method

Ryszard Staroszczyk

Institute of Hydro-Engineering of the Polish Academy of Sciences,
ul. Kościerska 7, 80-328 Gdańsk, e-mail: rstar@ibwpan.gda.pl

(Received April 01, 2011; revised May 17, 2011)

Abstract

The paper is devoted to numerical modelling of solitary wave propagation phenomena in shallow water of uniform depth. The problem governing equations are solved by applying a corrected smoothed particle hydrodynamics (SPH) method in which standard smoothing kernel functions are modified in such a way that so-called linear reproducing conditions for kernel approximations and their first-order spatial derivatives are satisfied. Numerical performance of the proposed SPH model has been verified by comparing its predictions with analytical results for a solitary wave travelling over the horizontal bottom. Also, the results obtained by applying the corrected SPH method and those given by the standard SPH method, with no kernel correction, are compared. Further, an impact of the solitary wave on a vertical rigid wall is investigated, and finally an interaction of two colliding solitary waves is considered.

Key words: solitary wave, non-linear wave interaction, meshfree Lagrangian method, smoothed particle hydrodynamics

Notations

a – reference particle label,
A – solitary wave amplitude,
b – neighbouring particle label,
c – solitary wave celerity,
g – acceleration due to gravity,
h – kernel smoothing length,
H – still water depth,
m – mass,
N – number of particles within a support domain,
p – pressure,
r – distance between two particles,

R – kernel support domain radius,
t – time,
$\boldsymbol{v}$ – velocity vector (with components u and v),
V – volume,
W – smoothing kernel function,
$\boldsymbol{x}$ – position vector (with components x and z),
η – free surface elevation,
ϱ – density.

1. Introduction

Since its origin (Lucy 1977, Gingold and Monaghan 1977), the Smoothed Particle Hydrodynamics (SPH) method has undergone significant improvements that have made it one of the most computationally effective discrete particle techniques used to solve problems in applied mechanics and engineering. Possessing all the advantages of a fully Lagrangian and meshless approach, the SPH method has the natural capability of treating the problems in which large displacements and deformations occur, or in which surfaces of material discontinuity develop and evolve.

Obviously, the SPH method has been also employed to solve a range of hydrodynamics problems, in particular those which are of importance to hydro- and off-shore engineering. For instance, Monaghan (1996) applied the method to investigate gravity currents and solitary waves, Lo and Shao (2002) analysed the run-up and run-down of solitary waves at a vertical wall and on a sloping beach, Colagrossi and Landrini (2003) treated the classical dam-break problem, including the analysis of water impact against a wall, Gómez-Gesteira et al (2005) simulated the phenomenon of a wave overtopping a flat rigid horizontal plate, Dalrymple and Rogers (2006) modelled problems of wave breaking on a sloping beach, Antoci et al (2007) analysed a fluid–elastic structure interaction problem, and most recently Ataie-Ashtiani et al (2008) considered the problem of the run-up of a tsunami wave on a sloping beach.

In the above papers, different variants of the SPH method have been applied. For example, in the papers of Monaghan (1996), Colagrossi and Landrini (2003) and Antoci et al (2007) the conventional SPH approach is followed in which water is treated as a weakly compressible fluid, in which pressure is related to fluid density by a constitutive law. In another group of formulations, represented by Lo and Shao (2002) and Ataie-Ashtiani et al (2008), water is modelled as an incompressible fluid, which is a common simplification in problems of gravity waves propagation. A typical feature of the latter formulations is the necessity to solve a Poisson equation for pressure at each time step in order to enforce the incompressibility constraint. This significantly increases the cost of computations, since the use of fast explicit time-stepping schemes, typical of the standard SPH method, is precluded.

An important aspect of the SPH implementation is the method of construction of an interpolation function (known in SPH as the smoothing kernel), used to approximate field variables in terms of quantities assigned to discrete particles. In a standard approach (Monaghan 1992, 1996), a single interpolating function, the same for all particles in a mechanical system considered, is applied, irrespective of mutual positions of the particles involved. By following this approach, a certain numerical error is generated, since the effects of an irregular scatter in particles distribution are not taken into account (the scatter is unavoidable as particles move past one another). The magnitude of this error considerably increases for particles situated near a boundary of the fluid domain. The reason for the above error to appear is the fact that the standard SPH method does not form a *partition of unity* (Belytschko et al 1998). To resolve this problem, a number of techniques have been developed to increase the accuracy of kernel approximation; usually these techniques originate from other discrete particle methods. It seems that the most consistent is a method in which the standard SPH kernel function is modified by multiplying it by a special correction function, so that the partition of unity is ensured. The principles on which the construction of such corrected kernels is based are the *consistency* and *completeness* of interpolating functions, and are known from the general theory of particle methods (Belytschko et al 1998). Such a combination of the standard SPH approach and the kernel correction technique is often referred to as the Corrected SPH (C-SPH) method, which has many features of a family of Moving Least-Square (MLS) particle methods. An improved accuracy of the corrected method, however, requires an additional computational effort, as the kernel function has to be calculated separately for each particle of the discrete system.

With regard to free-surface water flows, the corrected SPH approach has been applied by Colagrossi and Landrini (2003) and Dalrymple and Rogers (2006). The former authors employed one of the methods proposed by (Belytschko et al 1998), while the latter applied a kernel correction method known as the Shepard filtering. In both cases, only the correction of approximation functions has been carried out. In this paper, with the aim to further increase the accuracy of the SPH kernel interpolation, not only the approximation functions, but also their gradients (first-order spatial derivatives) are corrected. The proposed method is employed to simulate the behaviour of a solitary wave travelling in shallow water of uniform depth. In order to assess its reliability, the numerical SPH model is tested against first- and second-order analytical approximations to solutions of the Korteweg-de Vries equations describing non-linear waves in water of constant depth. Hence, it is shown how well the model is able to preserve an unchanged shape of the free surface profile and constant propagation velocity as the solitary wave propagates over a long distance, and the results predicted by the corrected method are compared with those given by the standard SPH method. Further, an impact of a solitary wave on a rigid vertical wall is investigated. The results of numerical calculations illustrate the evolution

of the free surface profile during an impact event, and show the variation of the maximum wave run-up on the wall with different wave amplitudes. Finally, an interaction of two solitary waves propagating in opposite directions is simulated, illustrating the changes in the free surface profile as the two waves collide.

The structure of the paper is as follows. In Section 2 governing equations which express the conservation and constitutive laws adopted in this work are presented, and initial conditions describing the free surface elevation and velocity and pressure fields in water generated by a solitary wave are given. Then, in Section 3, a brief outline of the SPH method is provided, followed by discrete formulations of differential equations describing the wave propagation problem considered. The section is concluded with a description of the time-integration method applied to solve the SPH equations. In the following Section, 4, results of numerical simulations are presented, and, finally, some conclusions are drawn in Section 5.

2. Problem Statement

In this work, water is treated as a weakly compressible inviscid liquid, and it is assumed that its motion is entirely due to the action of gravity. The fluid mass conservation balance, expressed in local form by the continuity equation, is given by

$$\frac{\mathrm{D}\varrho}{\mathrm{D}t} + \varrho \nabla \cdot \boldsymbol{v} = 0, \tag{1}$$

where $\mathrm{D}/\mathrm{D}t$ denotes the material (convected) time derivative, ϱ is the fluid density, t is time, $\boldsymbol{v}$ is the fluid velocity vector, and ∇ is the nabla operator. The linear momentum balance, expressing the Euler equation of motion, is defined by

$$\varrho \frac{\mathrm{D}\boldsymbol{v}}{\mathrm{D}t} = -\nabla p + \varrho \boldsymbol{b}, \tag{2}$$

where p is pressure, and $\boldsymbol{b}$ denotes the body force vector. In the problem considered here, the only body force is that due to the gravity.

The fluid motion is assumed to be barotropic, in which case the pressure is uniquely determined by the fluid density. In the standard SPH method, the following constitutive law relating the pressure p to density ϱ is usually adopted (Batchelor 1967):

$$p(\varrho) = p_0 \left[\left(\frac{\varrho}{\varrho_0} \right)^{\gamma} - 1 \right]. \tag{3}$$

In the latter equation, p_0 and ϱ_0 denote the reference pressure and density, respectively, and for water the typical value of the parameter γ is 7 (Colagrossi and Landrini 2003). The constitutive law (3) determines the speed of sound, c_s, as

$$c_s = \sqrt{\frac{\gamma\, p_0}{\varrho_0}}\,. \tag{4}$$

In practical implementations, the parameters p_0, ϱ_0 and γ are selected in such a way that the maximum local fluctuations of density ϱ around the reference value ϱ_0 are of order 1%. The idea of using the equation of state (3) for $p(\varrho)$, instead of applying the common water incompressibility condition $\varrho = \text{const}$, is that in this way one avoids the necessity of solving the Poisson equation for pressure. Therefore, fast explicit time-stepping algorithms can be employed in the SPH computations, instead of implicit schemes required when the Poisson equation has to be solved as part of the solution (Lo and Shao 2002, Ataie-Ashtiani et al 2008).

The boundary conditions, with which the continuity and motion equations (1) and (2) are solved, are adopted in the standard form, namely:

$$p = 0 \quad \text{on} \quad \Gamma_p\,, \quad \boldsymbol{v} \cdot \boldsymbol{n} = 0 \quad \text{on} \quad \Gamma_v, \tag{5}$$

where Γ_p denotes the fluid free surface, Γ_v denotes the solid boundary, and $\boldsymbol{n}$ is the unit vector normal to Γ_v. The initial conditions are defined by prescribing the free surface displacements and the velocity and pressure fields induced by a solitary wave at a given reference time. The latter fields are adopted as solutions of the Korteweg–de Vries (KdV) equations for plane non-linear waves propagating in shallow water of constant depth. In this work, use is made of the solutions derived by Wehausen and Laitone (1960) by applying a perturbation method. Referring to Fig. 1, showing the adopted coordinate system Oxz and relevant geometric parameters, two sets of relations defining the initial conditions for equations (1) and (2) are considered. These two sets represent, respectively, the first- and second-order approximations to the solitary wave solutions of the KdV equations.

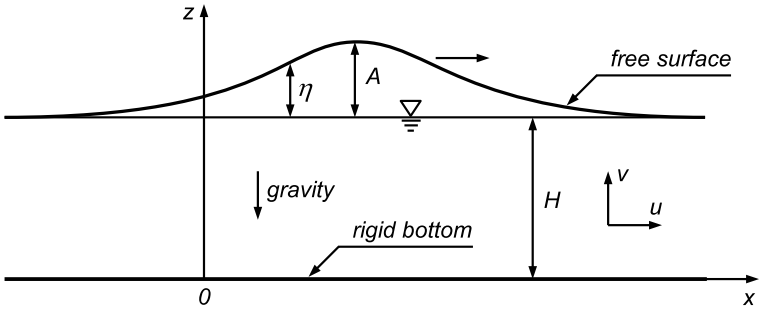

Fig. 1. Solitary wave problem definition: geometric parameters and coordinate axes

Assuming that the wave propagates in the direction of increasing x and its crest (the point of maximum free surface elevation) is at $x = 0$ at time $t = 0$, the first-order approximation is given by the expressions:

$$\frac{\eta(x,t)}{H} = \frac{A}{H}\,\mathrm{sech}^2\,\zeta + O\left(\frac{A}{H}\right)^2, \tag{6}$$

$$\frac{u(x,t)}{\sqrt{gH}} = \frac{\eta}{H} + O\left(\frac{A}{H}\right)^2, \tag{7}$$

$$\frac{v(x,z,t)}{\sqrt{gH}} = \sqrt{3}\,\frac{z}{H}\left(\frac{A}{H}\right)^{3/2} \operatorname{sech}^2\zeta\,\tanh\zeta + O\left(\frac{A}{H}\right)^{5/2}, \tag{8}$$

$$\frac{p(x,z,t)}{\varrho gH} = 1 + \frac{\eta - z}{H} + O\left(\frac{A}{H}\right)^2, \tag{9}$$

where $\operatorname{sech} x = 1/\cosh x$, η denotes the free surface elevation (measured with respect to the still water level $z = H$), u and v are the horizontal and vertical fluid particle velocities, and p is pressure. The argument of the hyperbolic functions, $\zeta(x,t)$, is defined by

$$\zeta = \frac{x - ct}{H}\sqrt{\frac{3}{4}\left(\frac{A}{H}\right)} + O\left(\frac{A}{H}\right)^{3/2}, \tag{10}$$

and the wave celerity (propagation velocity), c, is given by

$$\frac{c}{\sqrt{gH}} = 1 + \frac{1}{2}\left(\frac{A}{H}\right) + O\left(\frac{A}{H}\right)^2. \tag{11}$$

The second-order approximation to the solitary wave is given by the following set of formulae:

$$\frac{\eta(x,t)}{H} = \frac{A}{H}\operatorname{sech}^2\zeta - \frac{3}{4}\left(\frac{A}{H}\right)^2\left(1 - \operatorname{sech}^2\zeta\right)\operatorname{sech}^2\zeta + O\left(\frac{A}{H}\right)^3, \tag{12}$$

$$\begin{aligned}\frac{u(x,z,t)}{\sqrt{gH}} = {} & \frac{\eta}{H} - \frac{1}{2}\left(\frac{A}{H}\right)^2\left[1 + 6\left(\frac{z}{H} - 1\right) + 3\left(\frac{z}{H} - 1\right)^2\right]\operatorname{sech}^2\zeta + \\ & + \frac{1}{2}\left(\frac{A}{H}\right)^2\left[1 + 9\left(\frac{z}{H} - 1\right) + \frac{9}{2}\left(\frac{z}{H} - 1\right)^2\right]\operatorname{sech}^4\zeta + O\left(\frac{A}{H}\right)^3,\end{aligned} \tag{13}$$

$$\begin{aligned}\frac{v(x,z,t)}{\sqrt{gH}} = {} & \sqrt{3}\,\frac{z}{H}\left(\frac{A}{H}\right)^{3/2}\operatorname{sech}^2\zeta\,\tanh\zeta\,\left\{1 + \frac{A}{H}\left[\frac{1}{8} - \frac{z}{H} - \frac{1}{2}\left(\frac{z}{H} - 1\right)^2\right] + \right. \\ & \left. - \frac{1}{2}\left(\frac{A}{H}\right)\left[1 - 6\left(\frac{z}{H} - 1\right) - 3\left(\frac{z}{H} - 1\right)^2\right]\operatorname{sech}^2\zeta\right\} + O\left(\frac{A}{H}\right)^{7/2},\end{aligned} \tag{14}$$

$$\begin{aligned}\frac{p(x,z,t)}{\varrho gH} = {} & 1 + \frac{\eta - z}{H} - \frac{3}{4}\left(\frac{A}{H}\right)^2\left[\left(\frac{z}{H}\right)^2 - 1\right]\left(2\operatorname{sech}^2\zeta - 3\operatorname{sech}^4\zeta\right) + \\ & + O\left(\frac{A}{H}\right)^3,\end{aligned} \tag{15}$$

with the function $\zeta(x,t)$ defined by

$$\zeta = \frac{x - ct}{H}\sqrt{\frac{3}{4}\left(\frac{A}{H}\right)}\left[1 - \frac{5}{8}\left(\frac{A}{H}\right)\right] + O\left(\frac{A}{H}\right)^{5/2}, \tag{16}$$

and the wave celerity given by

$$\frac{c}{\sqrt{gH}} = 1 + \frac{1}{2}\left(\frac{A}{H}\right) - \frac{3}{20}\left(\frac{A}{H}\right)^2 + O\left(\frac{A}{H}\right)^3. \tag{17}$$

3. SPH Formulation

In the SPH approach, a continuum is discretized into a collection of particles, each of which carries, in a Lagrangian sense, information on all local physical properties of the medium under consideration. As no topological connectivity for neighbouring particles is required, the method has a fully meshless character, which gives it a great flexibility in dealing with large deformations. Field variables are approximated by using interpolation functions (smoothing kernels), which define weightings with which individual particles contribute to the value of a field function evaluated at a given spatial/material point. These functions are constructed in such a way that they have non-zero values only in a domain (usually a sphere or a circle) of a limited size, thus a number of particles involved in the interpolation is relatively small (typically between 20 to 50 in two-dimensional problems). The characteristic size of the above domain, known in the SPH as the *kernel support*, is described by a parameter R, which defines the *kernel radius*. All the particles which lie further than R from a given point do not contribute to the interpolation at that point (in other words, they do not interact with a particle currently being at that point). These features of the SPH interpolation method are sketched in Fig. 2.

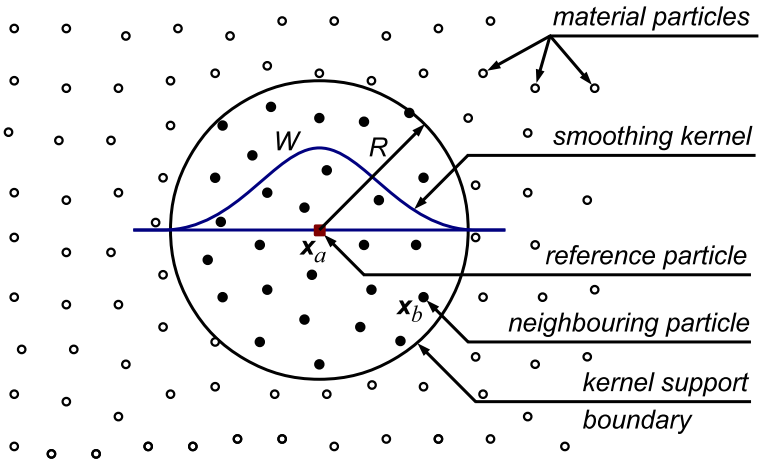

Fig. 2. Particle approximation involving material particles x_b (solid circles) located within a circular support domain of radius R around a reference particle x_a (solid square). Particles outside the support domain (empty circles) do not contribute to the approximation of field functions at x_a. W is the smoothing kernel function centred at x_a

Let $\boldsymbol{x}$ be the position vector, and a and b be labels of a pair of material particles. Then, the value of any field variable $f(\boldsymbol{x})$ at particle a (so-called reference particle), located at position $\boldsymbol{x}_a$, is evaluated by means of the kernel function, W, centred at this particle, by means of the formula

$$f(\boldsymbol{x}_a) = \sum_{b=1}^{N} V_b\, f_b\, W(r,h)\,, \tag{18}$$

where $f_b = f(\boldsymbol{x}_b)$ is the discrete value of f at particle b, V_b is the volume of particle b, and N is the number of particles within the kernel support. The smoothing kernel W is a function of two arguments. r is the distance between particles a and b, that is,

$$r = |\boldsymbol{x}_a - \boldsymbol{x}_b|, \tag{19}$$

and h is the so-called kernel smoothing length which defines the resolution of the discretization (an average number of particles involved in kernel interpolations).

Since the kernel W is a continuous function, it can be differentiated with respect to spatial coordinates to yield approximations to differential operators, needed to express physical laws in the SPH discrete forms. There is a variety of possible approximations to the gradient and divergence operators (Monaghan 1992, Li and Liu 2004). In this work, the gradient of a scalar function f at particle a is interpolated by

$$(\nabla f)_a = \varrho_a \sum_{b=1}^{N} m_b \left(\frac{f_a}{\varrho_a^2} + \frac{f_b}{\varrho_b^2} \right) \nabla_a W_{ab}\,, \tag{20}$$

while the divergence of a vector field $\boldsymbol{f}$ at particle a is interpolated by

$$(\nabla \cdot \boldsymbol{f})_a = -\frac{1}{\varrho_a} \sum_{b=1}^{N} m_b\, \boldsymbol{f}_{ab} \cdot \nabla_a W_{ab}\,, \tag{21}$$

with m_b denoting the mass of particle b. The following notations, typical of the SPH nomenclature, are used:

$$W_{ab} = W(|\boldsymbol{x}_{ab}|, h), \quad \boldsymbol{f}_{ab} = \boldsymbol{f}_a - \boldsymbol{f}_b\,, \tag{22}$$

and $\nabla_a W_{ab}$, defined by

$$\nabla_a W_{ab} = \frac{\boldsymbol{x}_{ab}}{|\boldsymbol{x}_{ab}|} \frac{\partial W(|\boldsymbol{x}_{ab}|, h)}{\partial |\boldsymbol{x}_{ab}|}\,, \tag{23}$$

denotes the gradient of the kernel function W taken with respect to the coordinates of particle a.

In terms of the interpolation formulae (20) and (21), the continuity and the momentum equations, (1) and (2) respectively, become

$$\frac{\mathrm{d}\varrho_a}{\mathrm{d}t} = \sum_{b=1}^{N} m_b \, \boldsymbol{v}_{ab} \cdot \nabla_a W_{ab} \tag{24}$$

and

$$\frac{\mathrm{d}\boldsymbol{v}_a}{\mathrm{d}t} = -\sum_{b=1}^{N} m_b \left(\frac{p_a}{\varrho_a^2} + \frac{p_b}{\varrho_b^2} \right) \nabla_a W_{ab} + \boldsymbol{b}_a \,. \tag{25}$$

The latter two forms are known to conserve exactly (Monaghan 1992, Li and Liu 2004) the mass and linear momentum of a system of material particles.

There are a number of kernel functions (Monaghan 1992, Liu and Liu 2003) that have been successfully applied in the SPH implementations, with the Gaussian and the cubic spline functions being probably the most often used. Here, a modified Gaussian kernel, proposed by Colagrossi and Landrini (2003), is employed which, in contrast to the common Gaussian distribution function, has a finite support. Hence, in two dimensions, the following expression is adopted:

$$W(r,h) = \frac{C}{h^2} \begin{cases} \left[\exp(-q^2) - \exp(-Q^2) \right], & q < Q, \\ 0, & q \geq Q, \end{cases} \tag{26}$$

where

$$q = r/h \quad \text{and} \quad Q = R/h, \tag{27}$$

and the normalizing factor C is given by

$$C = \frac{1}{2\pi \int_0^Q \left[\exp(-q^2) - \exp(-Q^2) \right] q \mathrm{d}q} \,. \tag{28}$$

Following the recommendation of Colagrossi and Landrini (2003), the kernel smoothing length h has been chosen to be equal to $R/3$, in which case $C = 1.0012356234/\pi$.

As said earlier, the standard SPH kernel does not form a partition of unity, since, in general, $\sum_{b=1}^{N} V_b W_{ab} \neq 1$ for a set of arbitrarily distributed discrete particles. This deficiency is particularly pronounced for particles located near/on the boundaries of a body, which is due to the fact that part of the particle kernel support domain (the part outside the body) is not filled with neighbouring particles. To restore the partition of unity, the standard SPH kernel is modified here by employing a formulation proposed by Belytschko et al (1998), in which both the SPH kernel functions and their gradients are corrected. Accordingly, for the two-dimensional case, the corrected kernel, $\widetilde{W}_{ab}$, and the two corrected components of the kernel

gradient, $(\nabla_a \widetilde{W}_{ab})_x$ and $(\nabla_a \widetilde{W}_{ab})_z$, are given in terms of the standard kernel functions W_{ab} as follows:

$$\begin{aligned} \widetilde{W}_{ab} &= (c_{11} + c_{12}\, x_{ab} + c_{13}\, z_{ab}) W^S_{ab}\,, \\ (\nabla_a \widetilde{W}_{ab})_x &= (c_{21} + c_{22}\, x_{ab} + c_{23}\, z_{ab}) W^S_{ab}\,, \\ (\nabla_a \widetilde{W}_{ab})_z &= (c_{31} + c_{32}\, x_{ab} + c_{33}\, z_{ab}) W^S_{ab}\,, \end{aligned} \tag{29}$$

where W^S_{ab} denotes the Shepard filtering function defined by

$$W^S_{ab} = \frac{W_{ab}}{\sum\limits_{b=1}^{N} V_b\, W_{ab}}\,, \tag{30}$$

$x_{ab} = x_a - x_b$, and $z_{ab} = z_a - z_b$. Note that the Shepard functions represent a partition of unity, since $\sum_{b=1}^{N} W^S_{ab} V_b = 1$ at any particle a in the domain, irrespective whether it is near, or far from, the boundary.

The nine coefficients $c_{\alpha\beta}(\boldsymbol{x})$ $(\alpha, \beta = 1, 2, 3)$ in (29) are determined by applying the completeness conditions for interpolating functions and their derivatives (Belytschko et al 1998). These conditions yield the matrix equation

$$\boldsymbol{c}^T = \boldsymbol{A}^{-1}, \tag{31}$$

in which $\boldsymbol{c}$ is the matrix of unknown coefficients $c_{\alpha\beta}$, and $\boldsymbol{A}$ is given by

$$\boldsymbol{A} = \sum_{b=1}^{N} V_b\, W^S_{ab} \begin{pmatrix} 1 & x_{ab} & z_{ab} \\ x_{ab} & x^2_{ab} & x_{ab}\, z_{ab} \\ z_{ab} & z_{ab}\, x_{ab} & z^2_{ab} \end{pmatrix}. \tag{32}$$

Note that the correction procedure requires, in two dimensions, the generation and subsequent inversion of the 3×3 matrix $\boldsymbol{A}$ for each discrete particle a. The resulting corrected kernel functions and their gradients are used to replace respective standard SPH counterparts in the equations of continuity and motion, expressed by relations (24) and (25).

Hence, the problem to be solved numerically can be summarized by the following set of first-order differential equations

$$\frac{\mathrm{d}\varrho_a}{\mathrm{d}t} = M_a\,, \quad \frac{\mathrm{d}\boldsymbol{v}_a}{\mathrm{d}t} = \boldsymbol{F}_a\,, \quad \frac{\mathrm{d}\boldsymbol{x}_a}{\mathrm{d}t} = \boldsymbol{U}_a\,, \tag{33}$$

where the third equation in (33) describes the trajectory of particle a. The interaction terms M_a and $\boldsymbol{F}_a$ in (33) are determined by the mass and momentum conservation balances. On account of (24) and (25), with the corrected forms of kernels and their

gradients applied instead of the standard ones, the terms M_a and $\boldsymbol{F}_a$ are expressed by

$$M_a = \sum_{b=1}^{N} m_b \, \boldsymbol{v}_{ab} \cdot \nabla_a \widetilde{W}_{ab} \,, \tag{34}$$

$$\boldsymbol{F}_a = -\sum_{b=1}^{N} m_b \left(\frac{p_a}{\varrho_a^2} + \frac{p_b}{\varrho_b^2} \right) \nabla_a \widetilde{W}_{ab} + \boldsymbol{b}_a \,. \tag{35}$$

The term $\boldsymbol{U}_a$ appearing in the third equation in (33) represents a corrected velocity of particle a, which is evaluated by employing the formula proposed by Monaghan (1992):

$$\boldsymbol{U}_a = \boldsymbol{v}_a + \varepsilon \sum_{b=1}^{N} \frac{m_a}{\bar{\varrho}_{ab}} \boldsymbol{v}_{ba} \widetilde{W}_{ab} \,, \quad \bar{\varrho}_{ab} = \frac{\varrho_a + \varrho_b}{2} \,. \tag{36}$$

The latter is known in the SPH literature as the XSPH correction, and its aim is to smooth out the velocity field around particle a by means of an average velocity of all neighbours b located within the kernel support of a. This helps to prevent inter-penetration of particles and ensures a more orderly and regular pattern of particles compared to the standard SPH approach. According to Monaghan, one should take $0 < \varepsilon < 1$ in (36); in the subsequent numerical simulations the value $\varepsilon = 0.5$ will be used.

The system of evolution equations (33), to be solved for all material particles of the discrete system, has been integrated in time by employing an explicit time-stepping scheme of a predictor–corrector type. Let a current time increment be defined by instants t^k and t^{k+1}, so that the time step length is $\Delta t = t^{k+1} - t^k$. Then, in the first prediction stage, the particle density, velocity and position are evaluated at the mid-step time $t^{k+1/2} = (t^k + t^{k+1})/2$ by

$$\begin{aligned} \varrho_a^{k+1/2} &= \varrho_a^k + \frac{\Delta t}{2} M_a^k \,, \\ \boldsymbol{v}_a^{k+1/2} &= \boldsymbol{v}_a^k + \frac{\Delta t}{2} \boldsymbol{F}_a^k \,, \\ \boldsymbol{x}_a^{k+1/2} &= \boldsymbol{x}_a^k + \frac{\Delta t}{2} \boldsymbol{U}_a^k \,. \end{aligned} \tag{37}$$

Then, using the latter half-step densities, the pressures $p_a^{k+1/2}$ are calculated from the constitutive law (3). These pressures, in turn, together with the predictions (37), yield the half-step values of $M_a^{k+1/2}$ and $\boldsymbol{F}_a^{k+1/2}$, determined by (34) and (35), and the half-step velocities $\boldsymbol{U}_a^{k+1/2}$, given by (36).

In the second stage of the current time step calculations, the mid-step values of the interaction terms are employed to calculate the respective values at the end of the time step, at $t = t^{k+1}$, according to the equations

$$\begin{aligned} \varrho_a^{k+1} &= \varrho_a^k + \Delta t\, M_a^{k+1/2}\,, \\ \boldsymbol{v}_a^{k+1} &= \boldsymbol{v}_a^k + \Delta t\, \boldsymbol{F}_a^{k+1/2}\,, \\ \boldsymbol{x}_a^{k+1} &= \boldsymbol{x}_a^k + \Delta t\, \boldsymbol{U}_a^{k+1/2}\,. \end{aligned} \tag{38}$$

Finally, the pressures p_a^{k+1} are updated by using the above end-step values of densities in (3), before the terms M_a^{k+1}, $\boldsymbol{F}_a^{k+1}$ and $\boldsymbol{U}_a^{k+1}$ are determined from (34), (35) and (39) to start the next time integration step.

In order to maintain the stability of computations, the time step length has been controlled by a Courant-Friedrichs-Levy-type condition expressed by

$$\Delta t \le \beta \frac{d}{c_s + v_{\max}}\,, \tag{39}$$

where d denotes an average inter-particle spacing, c_s is speed of sound given by (4), and $v_{\max}$ is the largest particle velocity, chosen here as the solitary wave celerity c defined by either (11) or (17). For the predictor–corrector time integration scheme applied in this work, the constant β should not exceed 0.3 (Colagrossi and Landrini 2003).

Besides the regularization of the velocity field by the XSPH correction method, it is also advisable to regularize the density field, as this helps to ensure consistency between particle mass, density and volume near the fluid free surface (Colagrossi and Landrini 2003, Dalrymple and Rogers 2006). Hence, in numerical computations, the density field is periodically smoothed out according to the formula

$$\varrho_a = \sum_{b=1}^{N} m_b\, \widetilde{W}_{ab}\,, \tag{40}$$

which is derived from equation (18) by setting $f = \varrho$ and replacing W_{ab} by its corrected form $\widetilde{W}_{ab}$ (recall that $m_b = V_b\, \varrho_b$). In the simulations, the results of which are presented in the next section, the above density regularization was carried out every twentieth time step.

4. Numerical Simulations

The numerical method described in the preceding section has been employed to simulate a plane problem of solitary waves propagation in water of uniform depth. In the simulations, an infinitely long layer of water has been replaced by a rectangular domain, with two vertical rigid walls confining the fluid at both sides of the rectangle. The length of the computational domain, L, has been chosen in

such a way that the initial free surface elevation induced by the solitary wave is sufficiently small at the vertical walls. Hence, these walls have been assumed at a distance of at least $10H$ from the wave crest, which means that the initial surface elevation at the walls is of order 10^{-3} of the wave height A. The initial water domain, the shape of which is determined by the profile of the free surface prescribed by either (6) or (12), has been discretized by adopting a regular grid of particles, with a uniform spacing d in the horizontal direction, and about the same spacing d along the vertical (the exact vertical spacing follows from the local free surface position). An example of the initial grid of discrete particles, near a wave crest, is given in Fig. 3.

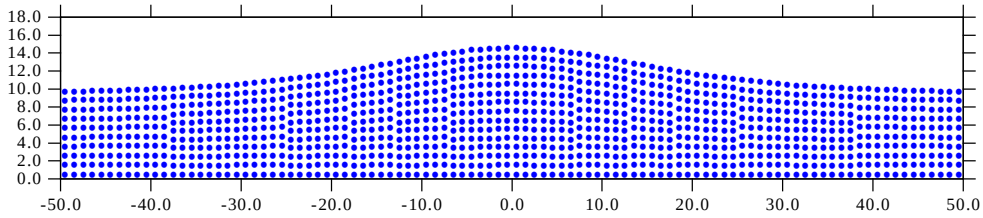

Fig. 3. Initial distribution of discrete particles. Labels along the axes show x- and z-coordinates in metres

At the solid boundaries (the horizontal bottom and the two vertical walls), free-slip conditions, defined by the second equation in (5), are enforced. There are a few methods available to implement boundary conditions in the SPH method. In this work a technique originated by Cummins and Rudman (1999), and slightly improved by Staroszczyk (2010), is used, in which so-called ghost particles are generated outside the walls to mirror physical properties of corresponding particles inside the water domain. Similar methods have been also used, among others, by Antoci et al (2007) and Ataie-Ashtiani et al (2008). However, this 'ghost particles' technique proves effective only in cases of simple convex fluid domains. Otherwise, when the fluid domain boundaries have a more complex geometry, more sophisticated methods ought to be employed. It seems that the technique developed very recently by Monaghan and Kajtar (2009), in which the boundaries are modelled by means of particles which exert repulsive forces on a fluid, has a potential of becoming a universal tool for treating such more complex boundaries.

The results presented below have been obtained for still water depth $H = 10$ m, and the wave amplitudes A ranging from 1 to 5 m. The physical parameters entering the equation of state (3) were $p_0 = 10^6$ Pa, $\varrho_0 = 10^3$ kg/m^3 and $\gamma = 7$. The evolution equations (33) were integrated with the time step length $\Delta t = 1 \times 10^{-3}$ or 2×10^{-3} s, depending on the particle spacing d, so that the condition (39) with $\beta = 0.3$ is satisfied.

At first, in order to assess the numerical efficiency of the proposed corrected SPH model, the simple problem of a single solitary wave travelling over the horizontal

bottom has been simulated. Hence, three amplitude ratios $A/H = 0.1$, 0.3 and 0.5, and the two cases of the initial free surface elevation, velocity and pressure fields in water given by the first- and second order approximations, defined by equations (6) to (11) and (12) to (17) respectively, are investigated. In the simulations, the water domain is adopted of length $L = 800$ m $= 80H$, and the initial inter-particle spacing is $d = 1$ m (10 particles along the water depth H). Therefore, the discrete system consists of 8066, 8136 and 8202 particles for the wave height ratios $A/H = 0.1$, 0.3 and 0.5, respectively. In all the computations, the SPH kernel support radius has been taken as $R = 4d$, and the kernel smoothing length parameter h, see (26) and (27), has been equal to $4d/3$. The maximum time of simulations is 50 s, during which the waves travel, see equations (11) and (17), the distances of about 50 to 60 water depths.

The three sets of plots in Fig. 4 illustrate free surface profiles of solitary waves moving to the right from the initial (wave crest) position at $x = 0$. Compared in the plots are the predictions of the proposed C-SPH method and the first-order analytical solutions of the KdV equations. It is seen that for the smallest wave considered, $A/H = 0.1$, there is a very good agreement between the numerical and analytical results, with the SPH profiles matching nearly exactly, both in terms of the height and the current position, those obtained analytically. For the wave height $A/H = 0.3$ still reasonable accuracy of the SPH solutions is maintained throughout the simulations, though it can be observed that the numerically obtained wave profiles are by several per cent higher, and a little slower, than the quantities predicted by the theory. On the contrary, the results given by the numerical method for the case of the largest waves, $A/H = 0.5$, clearly differ from the analytical ones, as significant discrepancies in the wave heights are observed, and also qualitative differences in the wave behaviour (the occurrence of negative free surface elevations η) are evident.

The plots in Fig. 5 present, in turn, the evolution of the free surface of water for the case of the initial wave profile given by the second-order approximations to the solution of the KdV equations. Again, the predictions of the C-SPH model are plotted against the analytical wave profiles, and additionally the results given by the standard (that is, not corrected) SPH method are shown. Comparing the corresponding plots in Fig. 4 and Fig. 5 it is seen that by taking the second-order solution as the initial wave profile in the simulations, better numerical results are achieved for the wave amplitudes $A/H = 0.1$ and $A/H = 0.3$, both in terms of the wave height and speed. Certainly, this has to be attributed to the fact that the second-order solution, for smaller ratios A/H, is by about one order of magnitude more accurate than the first-order analytical result — compare the respective expressions (6)–(17). On the other hand, it can be noted that the SPH predictions for the case of $A/H = 0.5$ are again unsatisfactory, which indicates that the waves of such a large height, due to their strongly non-linear behaviour, cannot be treated successfully by the proposed method, at least for the grid resolution and time step length applied in the present

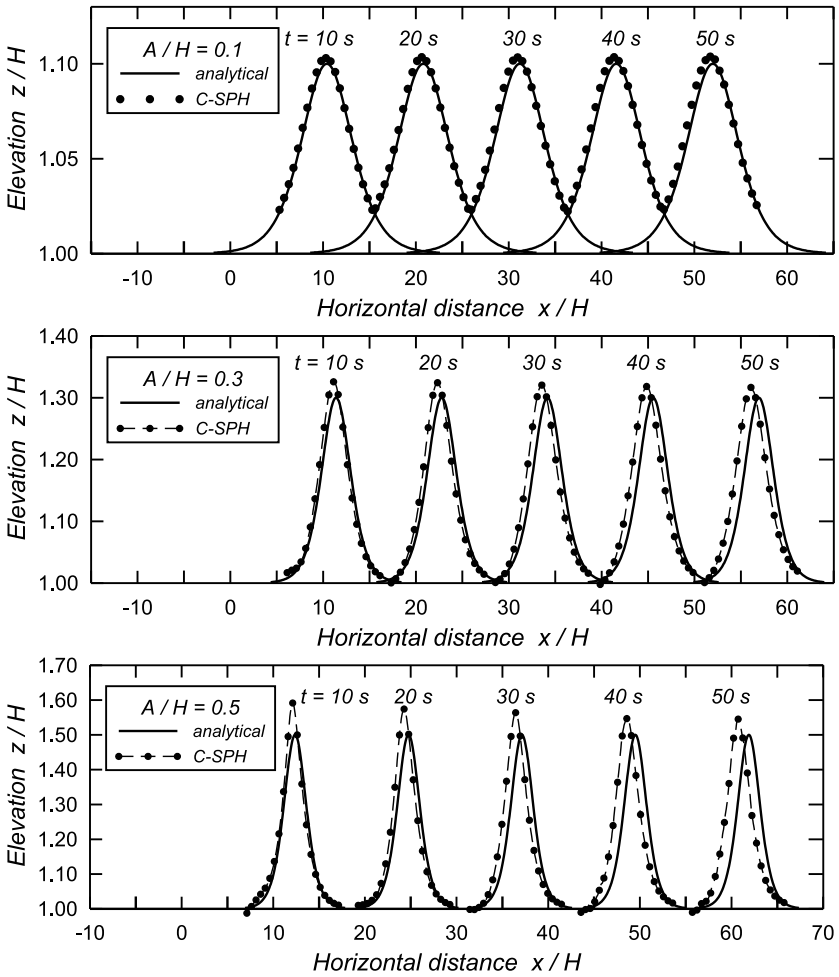

Fig. 4. Evolution of the water free surface for different dimensionless wave heights A/H, for the initial wave profile defined by the first-order solution of the KdV equation. Comparison of the numerical (C-SPH) results with analytical solutions

computations. The plots in Fig. 5 also show that the standard SPH approach, when compared with the corrected SPH method, yields the results of practically the same accuracy for the small waves defined by $A/H = 0.1$, slightly worse results for the medium-size waves $A/H = 0.3$ (with the differences increasing with increasing time t), and give definitely wrong results for the large waves $A/H = 0.5$. In the latter case, the numerically predicted wave starts to disintegrate as early as after about 20 s, that is, after the wave has travelled a distance of about $25H$.

Next, the problem of a solitary wave impacting on a rigid vertical wall has been examined numerically. In the SPH simulations, the computational water domain has a length $L = 25H$, and the fluid is represented by a grid of discrete particles

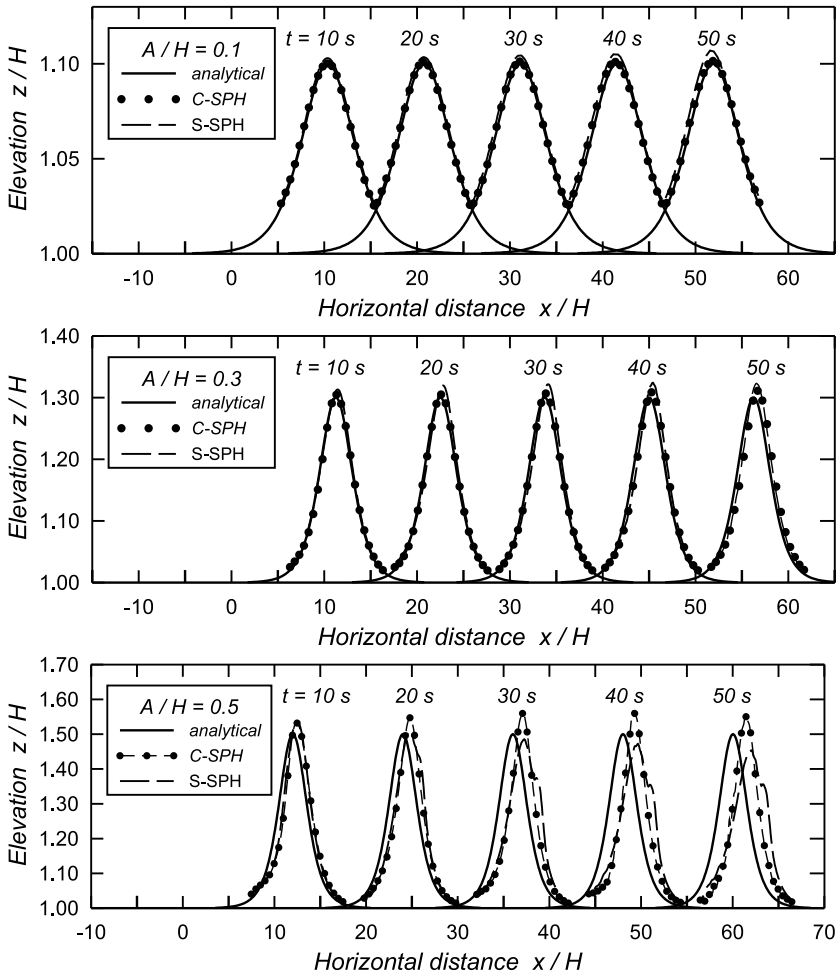

Fig. 5. Evolution of the water free surface for different dimensionless wave heights A/H, for the initial wave profile defined by the second-order solution of the KdV equation. Comparison of the corrected (C-SPH) and standard (S-SPH) results with analytical solutions

with an average spacing $d = 0.625$ m (16 particles along the still water depth H) in both x and z-directions. Hence, the model includes about 6800 particles. As the initial wave profile, the second order approximation defined by (12) has been used, together with accompanying expression (13) to (17) for other wave variables. The time integration of equations (33) has been carried out with the time increment $\Delta t = 1 \times 10^{-3}$ s.

The results obtained for a solitary wave of the height ratio $A/H = 0.3$ are presented in a series of plots in Fig. 6. The plots illustrate the evolution of the free surface elevation, starting from the instant $t = 0$, for a wave initially propagating to the right, then hitting the wall situated at $x/H = 10$ at the time $t \sim 9$ s, and, upon the

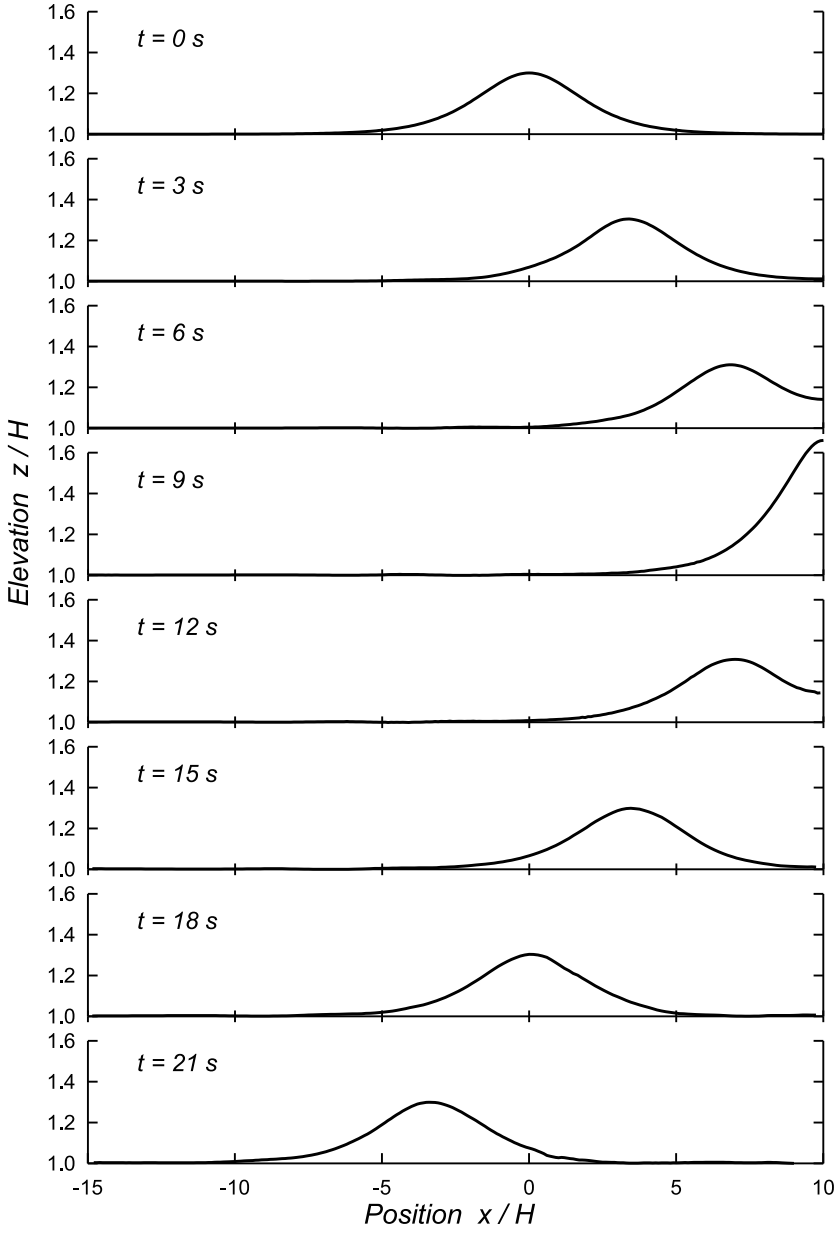

Fig. 6. Evolution of the free surface profile for a solitary wave of the amplitude $A/H = 0.3$ impacting at a vertical wall at $x/H = 10$

reflection, subsequently moving to the left. One can see in the plots that the reflected wave preserves its initial shape quite well, with satisfactorily smooth variation of the free surface profile throughout the simulations. However, with growing wave amplitudes, it is increasingly more difficult to maintain the smooth shape of the

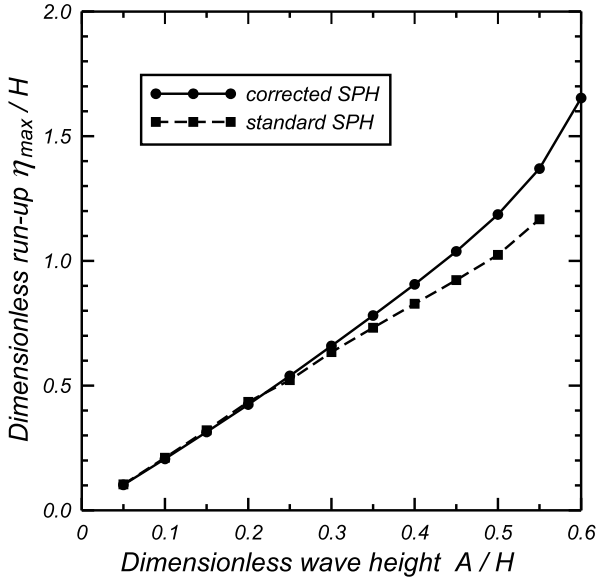

Fig. 7. Dependence of the maximum solitary wave run-up on the wave amplitude

reflected waves, though for the wave amplitude ratios as large as $A/H \sim 0.45$ still reasonable results are delivered by the present C-SPH method.

The above simulations have been conducted for wave height ratios A/H ranging from 0.05 to 0.6, with the aim to investigate the maximum wave run-up on the vertical wall. The results of calculations are given in Fig. 7, showing the dependence of the normalized run-up height, $\eta_{\max}/H$, on the dimensionless wave amplitude A/H. For reference, also the corresponding predictions of the standard SPH model are provided. It is seen that the two variants, corrected and standard, of the SPH method yield practically the same results for the wave amplitudes $A/H \lesssim 0.2$, with discrepancies becoming gradually more apparent as the ratio A/H increases beyond 0.2. Comparison of the results displayed in Fig. 7 with those collected by Lo and Shao (2002) and plotted in Fig. 3 of their paper shows that the predictions of the C-SPH model proposed here agree well with both experimental data and the results of other particle methods.

Finally, a collision of two solitary waves propagating in opposite directions has been simulated. Such a phenomenon gives rise to a complex non-linear interaction of the two waves, and therefore serves as a good test case for assessing the numerical robustness of any discrete method. Hence, the problem of two waves of different amplitudes, A_1 and A_2, approaching each other is examined in order to see how the wave profiles evolve during, and after, a collision event (the collision of two waves of the same amplitude is, essentially, equivalent to the wave reflection at a rigid wall, as illustrated in Fig. 6 above). The simulations have been performed by adopting a computational domain of a length $L = 50H$, with the initial wave crest positions of

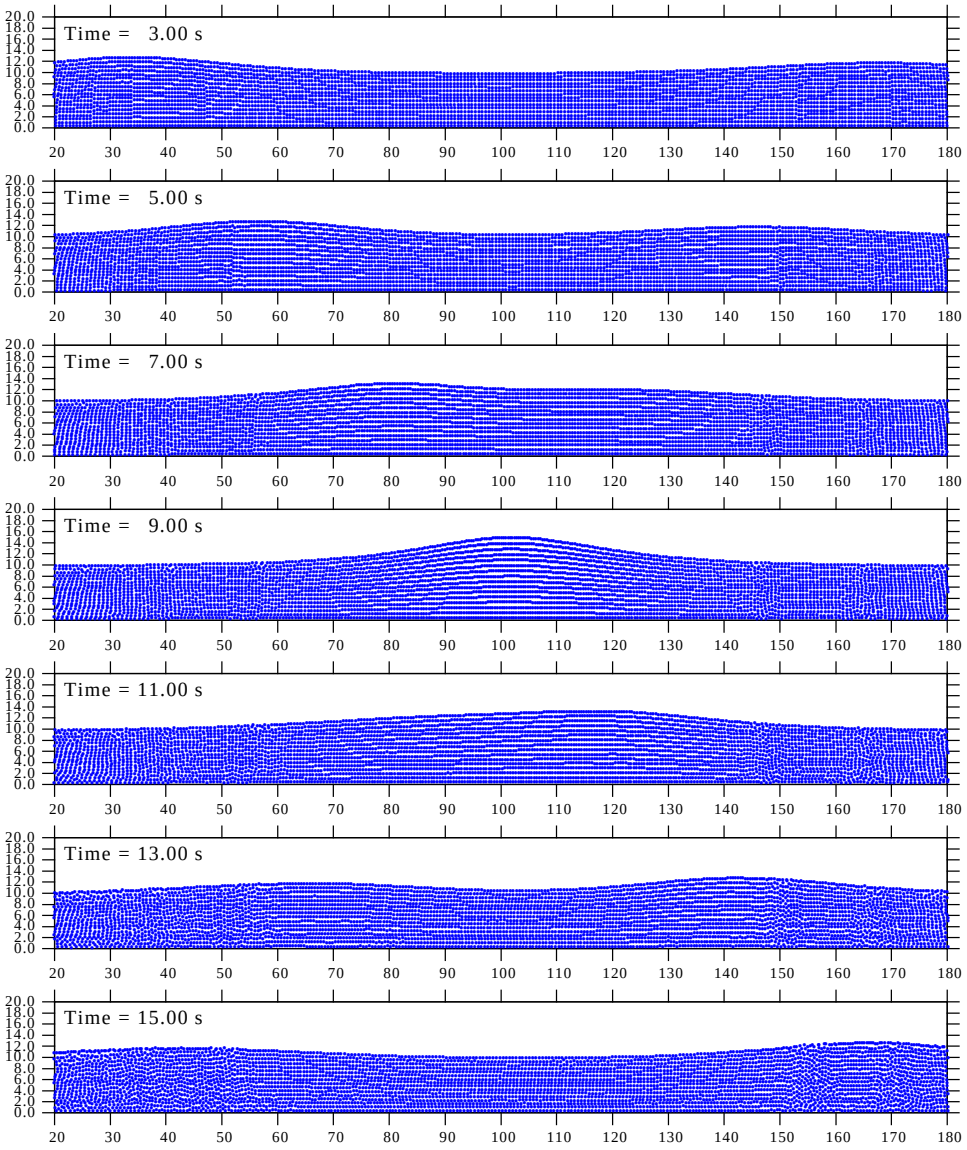

Fig. 8. Evolution of the discrete particle distribution during a collision of two solitary waves of the amplitudes $A_1/H = 0.3$ and $A_2/H = 0.2$. The larger wave moves from the left to the right

the two waves separated by a distance of $20H$. The same particle resolution as in the above-discussed problem of the wave impact against a wall is used, with 16 particles distributed uniformly along the water depth H, so that the model incorporates about 13 500 particles. Also, the same time increment $\Delta t = 1 \times 10^{-3}$ s has been used to integrate equations (33).

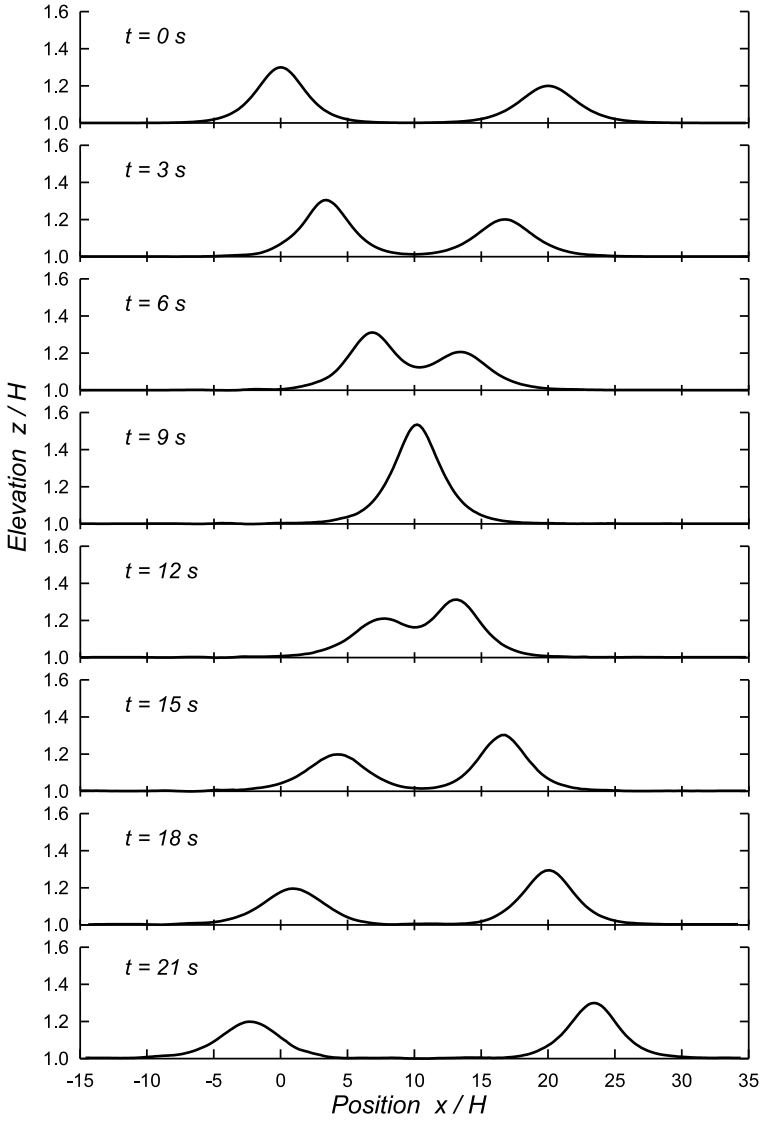

Fig. 9. Evolution of the free surface profiles of two colliding solitary waves of the amplitudes $A_1/H = 0.3$ and $A_2/H = 0.2$

The results of simulations are presented in Figures 8, 9 and 10. The first figure illustrates the evolution in time of the distribution of discrete particles in the central part of the computational domain, where the wave collision event takes place, in the case of waves of dimensionless amplitudes $A_1/H = 0.3$ and $A_2/H = 0.2$. The corresponding Fig. 9 displays the free surface profiles at successive time instants. We notice that the maximum free surface elevation at the collision time ($t \sim 9$ s) is larger than the sum of the two wave heights, which is an indication of the non-linear

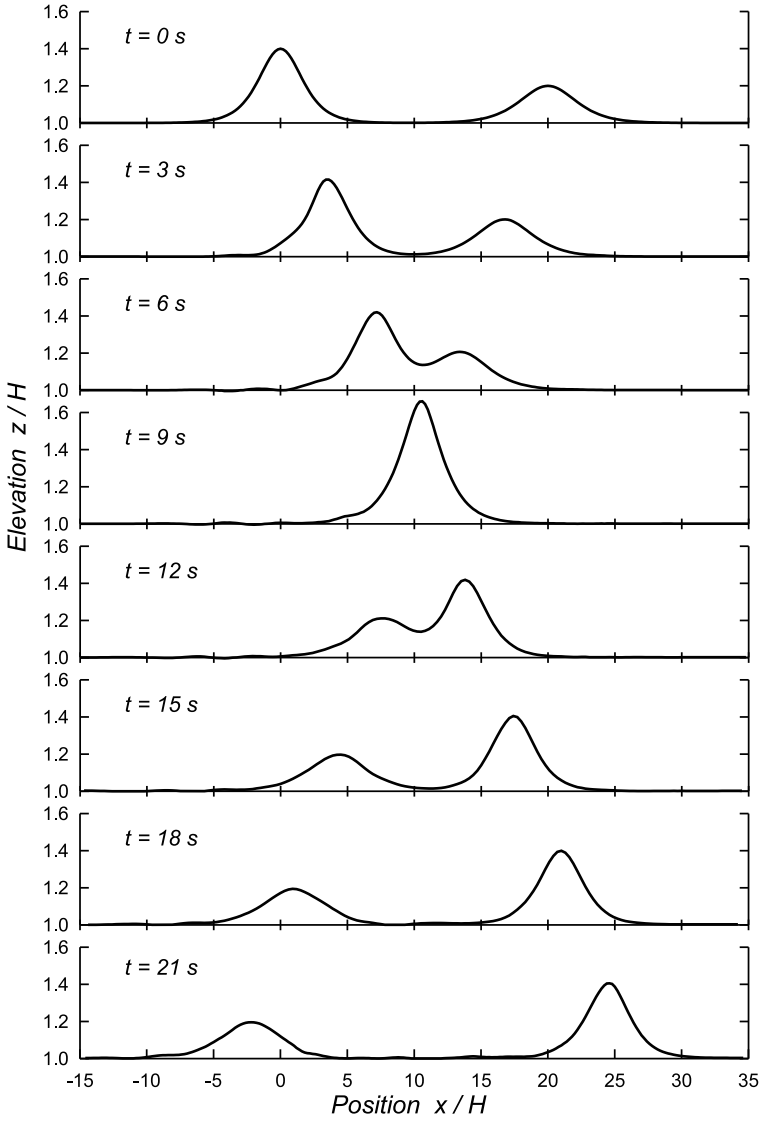

Fig. 10. Evolution of the free surface profiles of two colliding solitary waves of the amplitudes $A_1/H = 0.4$ and $A_2/H = 0.2$

character of the wave interaction mechanism. Further, one can observe that after the collision the two waves preserve their original shapes, with the free surface elevations varying in a smooth manner also for larger times, which demonstrates that the numerical model deals well with the solution of the problem considered.

A numerically more challenging case of the higher wave having a larger amplitude is illustrated in Fig. 10, displaying two colliding waves of amplitudes $A_1/H = 0.4$ and $A_2/H = 0.2$. Again, it seems that the results predicted by the C-SPH

model describe well the mechanism of the solitary wave interaction. Though, comparing the respective plots in Fig. 9 and 10 for larger times t, it is seen that some small oscillations of the numerical nature develop in the free surface profile behind the crest of the larger wave.

5. Conclusions

The results of simulations presented in Section 4 of the paper show that the corrected SPH method, in which the standard kernel function and its gradient are modified in order to enforce the partition of unity, deals well with the mechanics of solitary waves in shallow water. The method has proved to be capable of efficient modelling of strongly non-linear waves, the amplitude of which are as large as about 0.4 of the water depth. The predictions of the wave behaviour during two phenomena investigated — a solitary wave impact against a vertical wall and an interaction of two colliding waves — demonstrate that the model yields satisfactorily accurate and stable solutions. Of the two types of analytical approximations to the solution of the KdV equations used to prescribe the initial shape of the wave, the second-order approximation has proved to give better results, though the differences, in the case of small and medium-size waves, are not significant.

Comparisons of the results given by the corrected SPH method and those obtained by the standard SPH approach indicate that the two variants of the method yield practically the same results as long as the wave height does not exceed 0.2 of the still water depth. Therefore, in the case of such waves, it is recommended to use the standard SPH approach, since it is computationally much cheaper. On the other hand, larger solitary waves, the height of which is 0.2 and more of the water depth, can be treated with success only by applying the corrected SPH method, even though the latter turns out to be about three to four times computationally more expensive than its standard counterpart.

References

Antoci C., Gallati M. and Sibilla S. (2007) Numerical simulation of fluid–structure interaction by SPH. *Comput. Struct.* **85** (11-14), 879–890, DOI: 10.1016/j.compstruc.2007.01.002.

Ataie-Ashtiani B., Shobeyri G. and Farhadi L. (2008) Modified incompressible SPH method for simulating free surface problems. *Fluid Dyn. Res.* **40** (9), 637–661, DOI: 10.1016/j.fluiddyn.2007.12.001.

Batchelor G. K. (1967) *An Introduction to Fluid Mechanics*. Cambridge University Press, London.

Belytschko T., Krongauz Y., Dolbow J. and Gerlach C. (1998) On the completeness of meshfree particle methods. *Int. J. Numer. Meth. Eng.* **43** (5), 785–819, DOI: 10.1002/(SICI)1097-0207(19981115)43:5.

Colagrossi A. and Landrini M. (2003) Numerical simulation of interfacial flows by smoothed particle hydrodynamics. *J. Comput. Phys.* **191** (2), 448–475, DOI: 10.1016/S0021-9991(03)00324-3.

Cummins S. J. and Rudman M. (1999) An SPH projection method. *J. Comput. Phys.* **152** (2), 584–607, DOI: 10.1006/jcph.1999.6246.

Dalrymple R. A. and Rogers B. D. (2006) Numerical modeling of water waves with the SPH method. *Coastal Eng.* **53** (2-3), 141–147, DOI: 10.1016/j.coastaleng.2005.10.004.

Gingold R. A. and Monaghan J. J. (1977) Smoothed particle hydrodynamics: theory and application to non-spherical stars. *Mon. Not. R. Astron. Soc.* **181**, 375–389.

Gómez-Gesteira M., Cerqueiro D., Crespo C. and Dalrymple R. A. (2005) Green water overtopping analyzed with a SPH method. *Ocean Eng.* **32** (2), 223–238, DOI: 10.1016/j.oceaneng.2004.08.003.

Li S. and Liu W. K. (2004) *Meshfree Particle Methods*. Springer, Berlin.

Liu G. R. and Liu M. B. (2003) *Smoothed Particle Hydrodynamics: A Meshfree Particle Method*. World Scientific, Singapore.

Lo E. Y. M. and Shao S. (2002) Simulation of near-shore solitary wave mechanics by an incompressible SPH method. *Appl. Ocean Res.* **24** (5), 275–286, DOI: 10.1016/S0141-1187(03)00002-6.

Lucy L. B. (1977) A numerical approach to the testing of the fission hypothesis. *Astron. J.* **82** (12), 1013–1024.

Monaghan J. J. (1992) Smoothed particle hydrodynamics. *Annu. Rev. Astron. Astrophys.* **30**, 543–574, DOI: 10.1146/annurev.aa.30.090192.002551.

Monaghan J.J. (1996) Gravity currents and solitary waves. *Physica D* **98** (2-4), 523–533.

Monaghan J. J. and Kajtar J. B. (2009) SPH particle boundary forces for arbitrary boundaries. *Comput. Phys. Comm.* **180** (10), 1811–1820, DOI: 10.1016/j.cpc.2009.05.008.

Staroszczyk R. (2010) Simulation of dam-break flow by a corrected smoothed particle hydrodynamics method. *Arch. Hydro-Eng. Environ. Mech.* **57** (1), 61–79.

Wehausen J. V. and Laitone E. V. (1960) Surface waves. In: *Encyclopedia of Physics* (ed. S. Flügge), vol. IX, Springer, Berlin, pp. 446–778.